Journal of Crystal Growth 643 (2024) 127816

Contents lists available at ScienceDirect

Journal of Crystal Growth

journal homepage: www.elsevier.com/locate/jcrysgro

Synthesis and properties of quasi-one-dimensional BiSBr crystals via the Bridgman-Stockbarger technique

R. Sereika [a,*], Š. Varnagiris [b], M. Urbonavičius [b], R. Žaltauskas [a], D. Milčius [a,b]

[a] Vytautas Magnus University, K. Donelaičio Str. 58, LT-44248 Kaunas, Lithuania
[b] Center for Hydrogen Energy Technologies, Lithuanian Energy Institute, LT-44403 Kaunas, Lithuania

ARTICLE INFO

Communicated by Matthias Bickermann

Keywords:
BiSBr
Bridgman-Stockbarger technique
X-ray diffraction
X-ray photoelectron spectroscopy
Raman

ABSTRACT

This investigation details the synthesis and comprehensive characterization of semiconducting bismuth sulfobromide (BiSBr) crystals, emphasizing their structural and optoelectronic properties. Using the Bridgman-Stockbarger technique, we synthesized large, high-quality BiSBr crystals, which were systematically examined through techniques such as X-ray diffraction, X-ray photoelectron spectroscopy, and Raman spectroscopy. These methods confirmed the crystals' quasi-one-dimensional structure and their exceptional stability, demonstrating an absence of surface oxidation, which is a significant advantage for optoelectronic applications. The study establishes a correlation between the crystals' unique structural characteristics and their enhanced optoelectronic properties, particularly regarding light absorption and thermal conductivity, thereby underscoring their potential in sustainable energy technologies. This work not only advances our understanding of BiSBr as a promising material for optoelectronic devices, but also paves the way for future research into its practical applications in energy conversion and storage systems.

1. Introduction

Foundational studies have shown that bismuth sulfobromide (BiSBr) crystallizes in an orthorhombic structure characterized by infinite double chains. This structure was first detailed by G. P. Voutsas and P. J. Rentzeperis in 1984, building upon earlier observations by E. Dönges [1–3] and has been instrumental in guiding further research into its potential applications. While related compounds SbSI and SbSBr from the same $A^{V}B^{VI}C^{VII}$ family are recognized for their ferroelectric properties [4–6], BiSBr has been increasingly noted for its suitability in optoelectronic applications due to its unique quasi-one-dimensional structure, inherent electronic characteristics, and notable thermoelectric performance [7–10].

BiSBr's distinctive orthorhombic crystal structure significantly enhances its light absorption capabilities, which is crucial for applications such as photovoltaics. This positions BiSBr as a formidable candidate for various optoelectronic devices. Theoretical studies, primarily *ab initio* calculations, have detailed the optical properties of BiSBr, revealing intricate aspects of its dielectric function, absorption coefficients, and reflectivity across a broad energy spectrum. These investigations underscore the anisotropic behavior of BiSBr's optical spectra, further demonstrating its suitability for high-efficiency photovoltaic applications due to its favorable band gap and robust optical absorption characteristics [11–13]. These properties originate from electronic transitions between valence and conduction bands, which are heavily influenced by orbital hybridization. This hybridization enhances the covalent-ionic character of its bonding, significantly impacting its electronic properties [12,14]. Such electronic structural features not only contribute to its high photoconductivity, but also enhance its potential in electromechanical applications. Furthermore, emerging studies on BiSX materials have highlighted the tunability of their band gaps through compositional adjustments, offering enhanced control over their optoelectronic properties [15]. Compositionally tunable BiSX nanocrystals with high absorption coefficients and indirect band gaps ranging from approximately 1.5 to 2.5 eV have been synthesized, demonstrating quantum efficiencies above 10 percent across the entire visible light spectrum in photoelectrode applications [16]. These advancements underscore the potential of BiSBr and its derivatives for fabricating high-performance devices, further emphasizing the critical role of these less toxic inorganic ns^2-type lead-free materials in developing sustainable energy solutions [14–18].

In response to the renewed interest in this material and its promising

* Corresponding author.
E-mail address: raimundas.sereika@vdu.lt (R. Sereika).

https://doi.org/10.1016/j.jcrysgro.2024.127816
Received 15 May 2024; Received in revised form 10 July 2024; Accepted 10 July 2024
Available online 14 July 2024

applications, the present study focuses on the synthesis of large, high-quality BiSBr crystals using the Bridgman-Stockbarger method, accompanied by comprehensive experimental spectroscopic analyses, including X-ray diffraction (XRD), X-ray photoelectron spectroscopy (XPS), and optical Raman spectroscopy.

2. Experimental methods

The BiSBr crystals were grown using the vertical Bridgman–-Stockbarger technique. Stoichiometric amounts of $BiBr_3$ (99.998 % trace metals basis), Bi (99.999 %), and S (99.99 %) with a total mass of 25 g were placed in a quartz ampoule (150 mm in length and 15 mm in inner diameter) that was subsequently evacuated and sealed. One end of the ampoule had a specially shaped constriction to facilitate the formation of crystal seeds (see Fig. 1). The mixing of the loaded materials was conducted in a continuously rolling furnace where the temperature was raised to 950 K at a rate of approximately 0.25 K/min. The sublimation at high temperature took 3 days, and then the temperature was reduced at the same rate to 400 K. The entire process took approximately seven days. Prior attempts to grow crystals using a mixture of $BiBr_3$ and Bi_2S_3 resulted in an explosion during the initial heating phase, highlighting the sensitivity of the materials involved. After the sublimation process, the ampoule was removed at room temperature and transferred to a vertical furnace. The ampoule was lowered in the furnace at a speed of 0.8 mm/h, passing through the hot zone and subsequently entering the cool zone. Crystallization started at the lower part of the ampoule and gradually developed until the ampoule had descended completely. The temperature in the center of the furnace was maintained at 720 K. The overall growth process took about two weeks.

For the structural analysis, part of the resulting ingot of BiSBr was ground into a powder. The powder XRD measurement was performed using the SmartLab (Rigaku) diffractometer. The data were collected at room temperature and refined using the GSAS-II software package [19]. XPS was used to investigate the surface composition and chemical state of the elements within cleaved pieces of BiSBr. XPS spectra were acquired at room temperature by using a PHI Versaprobe 5000 spectrometer. The photoelectrons were excited using monochromatized 1486.6 eV Al K_α radiation, with a 25 W beam power, a 100 μm beam size, and at a 45° measurement angle. Sample charging was compensated using dual neutralization system consisting of a low-energy electron beam and an ion beam. The random C 1*s* line at a binding energy of 284.6 eV was used for correction of the charging effects. After background subtraction, a non-linear least squares curve fitting routine with a pseudo-Voigt function was used for the analysis of XPS spectra. The optical Raman spectra were measured on a Renishaw spectrometer with a red laser, which gave the best signal. The data collection time was 15 s and a laser power of 7 mW was set to take the spectrum. All experiments were conducted on samples from the same preparation batch.

3. Results and discussion

Powder XRD measurements confirm that BiSBr, obtained by using the Bridgman–Stockbarger technique, adopts an orthorhombic structure (space group *Pnma*, no 62) with four molecules (12 atoms) per unit cell. Fig. 2 shows the XRD pattern analyzed using Rietveld refinement, which involved fitting the experimental data to a theoretical model. This refinement process enabled the precise determination of the lattice parameters and atomic positions. The unit cell parameters $a = 8.1267 \pm 0.002$ Å, $b = 9.8154 \pm 0.002$ Å, and $c = 4.0587 \pm 0.002$ Å (for more details, see Table 1). This coincides with earlier reports on the structure of BiSBr, with slight variations likely affected by the synthesis method [3,10,15,16]. The density was estimated to be 6.58 g/cm^3, indicating that the material is denser than many traditional semiconductor materials used in microelectronics. As can be seen from Fig. 1(b), the crystallographic *c*-axis is within the direction of the BiSBr chains; this is typical for this class of materials and can be beneficial for certain optoelectronic properties such as anisotropic electrical conductivity and optical absorption. The cleaved crystals exhibit a shiny metallic luster, suggesting a smooth cleavage plane, which is often a sign of high crystal quality. Here, the weak van der Waals forces between the chains facilitate easy cleavage, as evidenced by the smooth surfaces of the crystals. The macroscopic image provides visual evidence of the one-dimensional growth habit. Such morphologies are known to influence the electrical transport along different crystallographic directions and can be exploited in directional charge transport applications. In addition, a notable feature of the BiSBr structure is the presence of a lone pair on the bismuth ion. While this lone pair does not participate directly in bonding, it

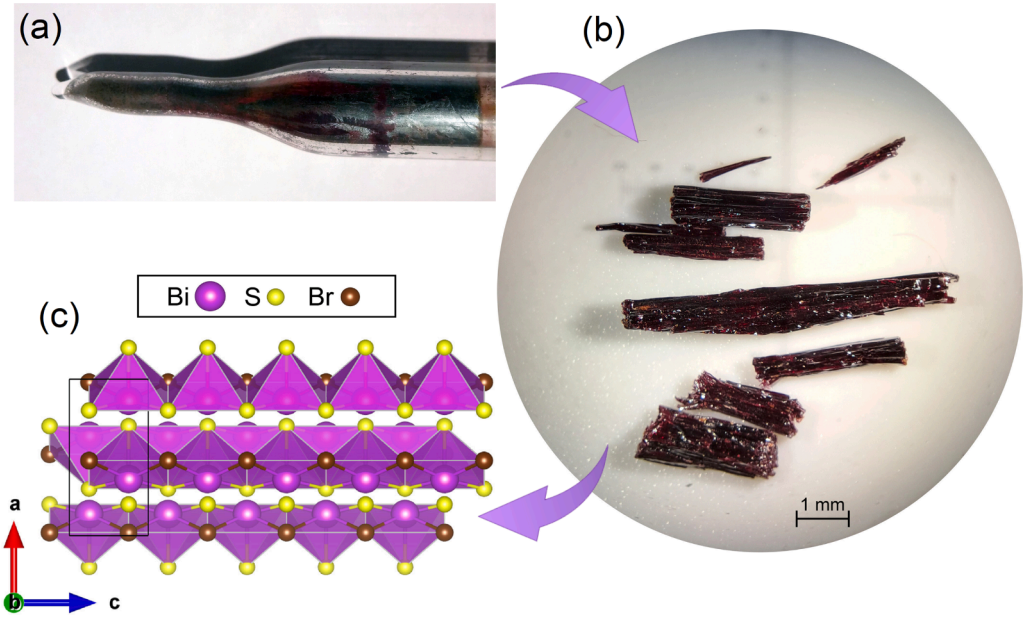

Fig. 1. Visual and structural view of the BiSBr crystal. (a) An ingot in a quartz ampule obtained from vertical Bridgman growth. (b) Microscope image showing pieces of the crystal that were cut and cleaved along the translational direction of the Bridgman growth. (c) Crystal structure of BiSBr highlighting chains along the *c*-axis and the square pyramidal coordination of Bi atoms.

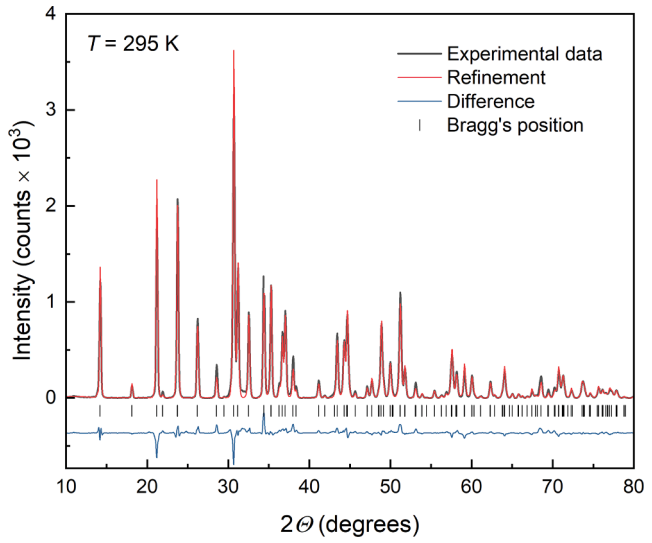

Fig. 2. X-ray diffraction pattern of the BiSBr powders along with the Rietveld analysis. The black line represents the experimental data, the red line represents the refinement, the blue line shows the difference between the experimental data and the refinement, and the vertical bars indicate Bragg's positions of the orthorhombic *Pnma* phase. (For interpretation of the references to colour in this figure legend, the reader is referred to the web version of this article.)

Table 1
The Rietveld refinement results of the BiSBr lattice parameters and atomic positions.

Atom	Space group *Pnma* (Wyckoff positions 4c), T=295 K.		
	a = 8.1267 ± 0.002 Å, b = 9.8154 ± 0.002 Å, c = 4.0587 ± 0.002 Å, $\alpha = \beta = \gamma = 90°$, V=323.75 Å^3, Z=4		
	x	***y***	***z***
Bi	0.3594(5)	0.6306(5)	0.7500
S	0.3193(5)	0.4411(5)	0.2500
Br	0.5068(5)	0.8195(5)	0.2500

significantly influences the system by affecting bond lengths and angles, thereby impacting the electronic and optical properties of the material. Typically, lone pairs in small coordination polyhedral with strong covalent bonds tend to be active, and their activity often increases with the distortion of the local environment. However, in similar bismuth compounds like BiSI and BiSeI, lone pairs have been found to be relatively diffused, and thus weakly stereoactive, due to the scalar-relativistic contraction of the Bi-6*s* shell, which results in only minor pseudo-octahedral distortions in the lattice [20]. In bismuth oxyhalides (BiOF, BiOCl, BiOBr, and BiOI structures), the Bi-6*s* lone pair makes only a minor contribution to the top of the valence band and is not considered stereoactive [21]. Meanwhile, preliminary data suggest that the stereochemical activity of the bismuth lone pair in BiSBr may be significant; this is being further investigated for its potential impact on the material's properties [7].

The crystal structure model shown in Fig. 1(c) further illustrates the atomic arrangements within the BiSBr lattice. In this structure, Bi atoms form a backbone for the double chains with bridging S atoms, while Br atoms are situated externally to the chains. The observed strong Bi-S and Bi-Br bonds reflect a hybrid covalent-ionic character; the Bi-S bonds are predominantly covalent, providing a high degree of crystallographic order, while the Bi-Br bonds exhibit a more pronounced ionic character, as indicated by the ionicity factor [12]. This hybrid bonding nature contributes to the material's unique optoelectronic properties and high photoconductivity. Furthermore, the optical properties are profoundly influenced by local field effects and excitonic interactions, which significantly affect the excitonic stabilization energy and thus impact the absorption spectrum, critical for applications that require efficient light absorption [13].

In general, to balance the charge, BiSBr with 1:1:1 stoichiometry should be formed from a trivalent cation with divalent and monovalent anions, respectively. Here, we used XPS methods to define the chemical state and related peculiarities of the BiSBr crystal. Fig. 3 presents the XPS peaks for Bi 4*d*, Bi 4*f*, S 2*s*, S 2*p*, and Br 3*d*, which were collected at room temperature. The Bi 4*d* spin–orbit doublet appears at binding energies (BEs) of 442.8 eV for Bi $4d_{5/2}$ and 466.1 eV for Bi $4d_{3/2}$, as depicted in Fig. 3(a). These BEs closely resemble those reported for bismuth chalcogenide compounds, specifically analogous to values observed in Bi_2S_3. [22,23]. Such alignment implies that these peaks are indicative of bismuth-sulfur bonding. Additionally, prominent Bi spin–orbit doublet peaks, Bi $4f_{7/2}$ and Bi $4f_{5/2}$ are observed at BEs of 159.6 and 164.9 eV, respectively (Fig. 3(b)). The BEs for Bi 4*f* align well with those reported for ternary Bi-containing compounds, corroborating the presence of Bi^{3+} species [10,16,24,25]. The S $2p_{3/2}$ and S $2p_{1/2}$ spin–orbit components are identified with BEs of 161.9 eV and 163.2 eV, aligning with typical sulfide values, suggesting a S^{2-} state for sulfur in BiSBr. The S 2*s* peak at 227.1 eV further supports this assignment. Similarly, the Br $3d_{5/2}$ and Br $3d_{3/2}$ spin–orbit doublet, with BEs of 68.8 eV and 69.8 eV, respectively, are consistent with Br^- species.

It is noteworthy that, for crystals such as BiSI and SbSI, which are typically grown from the vapor phase, significant shifts in core-level binding energies have been observed, contingent on the crystallographic plane examined. This effect is linked to the differential potential encountered by surface atoms compared to those in the bulk, owing to the surface atoms' diminished coordination numbers. Such variances lead to corresponding changes in their core-electron binding energies, as evidenced by previous studies [25,26]. However, our XPS analysis highlights the remarkable surface stability of BiSBr, a characteristic that differentiates it from similar materials that frequently undergo surface oxidation, as demonstrated in SbTeI case [27]. In accordance with prior research that emphasizes the material's air and photo-stability [8], our findings affirm that the BiSBr surface remains unaltered and free from oxidation.

Fig. 4 shows the Raman spectrum of BiSBr under ambient conditions. The measurements on crystals reveal well-defined modes that surpass those observed in thin films [8,10], providing more intricate details. All experimentally observed modes lie in the frequency range up to 300 cm^{-1}. According to factor-group analysis, the orthorhombic *Pnma* space group at the Brillouin zone center has 36 normal modes: three acoustic vibrations ($B_{1u} + B_{2u} + B_{3u}$) and 33 optical vibrations ($6_{Ag} + 3B_{1g} + 6B_{2g} + 3B_{3g} + 3A_u + 5B_{1u} + 2B_{2u} + 5B_{3u}$). Among the optical modes, 18 are Raman-active. Earlier studies indicated a very close similarity among Raman spectra of $A^{V}B^{VI}C^{VII}$ chain-type compounds, suggesting that the crystalline chain-type structure remains unchanged by the elemental substitutions [28]. The results are then interpreted in terms of the mass change based on a semi-ionic model. Notably, these systems with substitutional elements exhibit two-mode behavior in Raman spectra, which is indicative of strong covalent bonding within the structures that lead to localized vibrational states. For example, the replacement of trivalent atoms in $Bi_xSb_{1-x}SI$ and $Bi_xSb_{1-x}SeI$ solid solutions demonstrate the presence of both end-member highest frequency modes instead of a singular, averaged mode [29–32]. The prominent highest frequency mode in BiSBr is located at 286.7 cm^{-1} and is attributed to the strong covalent bonding between Bi and S atoms within the structure. Consequently, the BiSBr framework can be conceptualized as comprised of covalent bismuth sulfide units $(Bi^{3+}S^{2-})^+$, which are charge-balanced by bromine ions Br^-. Thus, Raman-active modes involving covalent Bi-S bonds are expected to exhibit significant shifts in frequency if Bi or S are substituted. Conversely, replacing monovalent atoms does not result in a two-mode behavior [33], indicating weaker bonds between Bi and Br that do not significantly affect the vibrational dynamics of the crystal lattice. This underscores the potential for

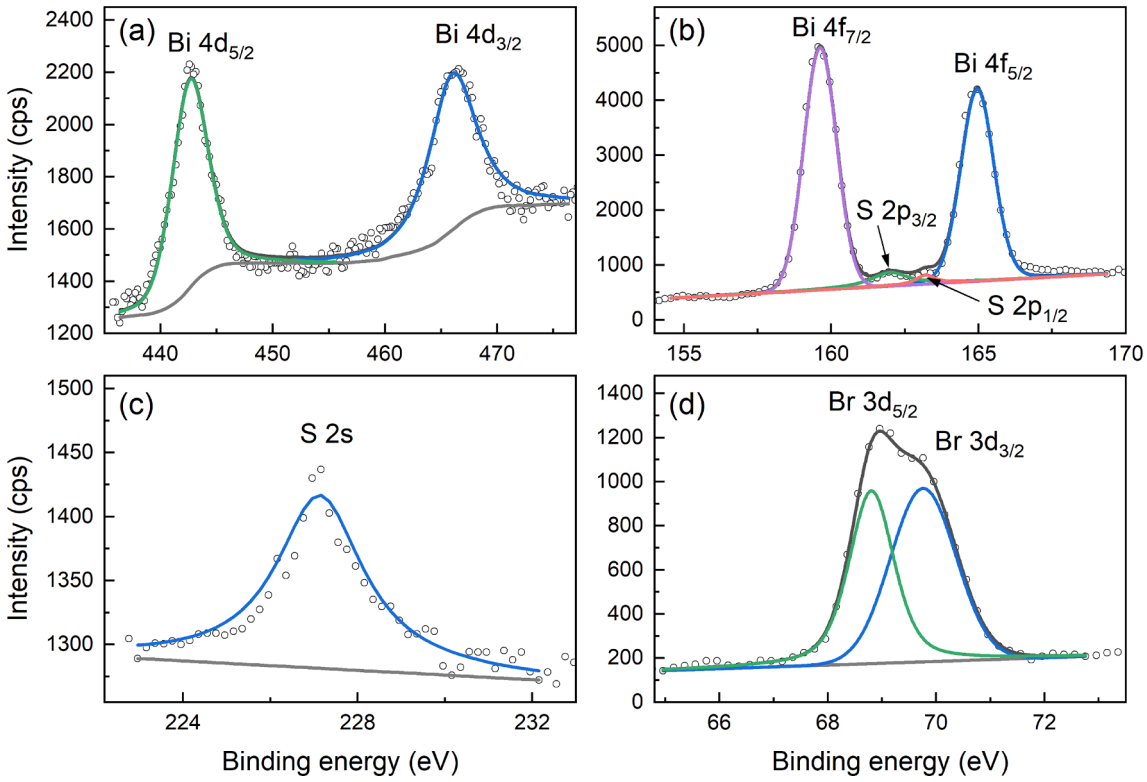

Fig. 3. XPS spectra of a BiSBr crystal. (a) Bi 4*d* core level showing peaks for Bi $4d_{5/2}$ and Bi $4d_{3/2}$. (b) Overlapping Bi 4*f* and S 2*p* core levels with identified peaks for Bi $4f_{7/2}$, Bi $4f_{5/2}$, S $2p_{3/2}$, and S $2p_{1/2}$. (c) S 2 *s* core-level spectrum. (d) Br 3*d* core level displaying peaks for Br $3d_{5/2}$ and Br $3d_{3/2}$. The solid lines represent the peak fitting results, used to determine the binding energies and intensities of the core levels.

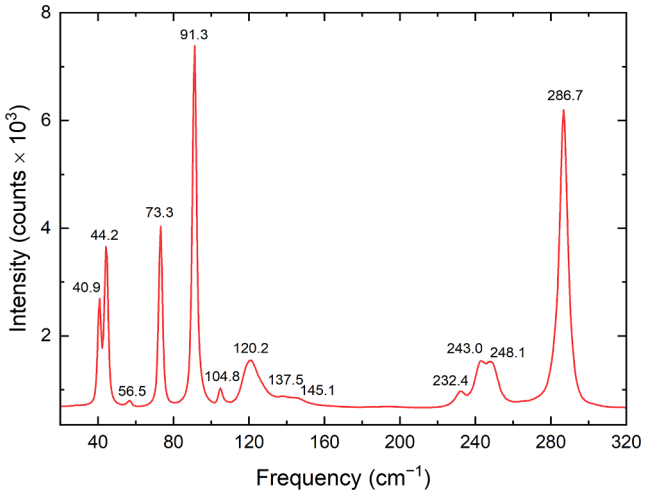

Fig. 4. Raman spectrum of BiSBr crystal in the frequency range from 20 to 320 cm^{-1}.

strategic cation/anion substitutions to fine-tune the band gap.

The vibrational behavior and mode stability in BiSBr are corroborated by theoretical studies of the phonon dispersion spectrum, which indicate only positive frequencies throughout the Brillouin zone, confirming the dynamical stability of BiSBr [7]. Moreover, the absence of a substantial gap between the acoustic and optical phonon modes, as documented in the literature, suggests a coupling between these two types of vibrations. The acoustic-optical phonon coupling has significant implications for the material's thermal properties, potentially suppressing heat transport and consequently affecting the thermal conductivity of BiSBr. The restriction of phonon transmission, due to weak van der Waals forces in the interchain regions – an indicator of low thermal conductivity – underscores BiSBr's suitability for thermoelectric applications.

While the Raman spectrum provides valuable experimental data, the complete correlation of observed Raman peaks to specific vibrational modes remains challenging due to the lack of comprehensive theoretical assignments in the current literature. Detailed theoretical modeling is essential to fully understand the lattice dynamics and accurately assign the vibrational modes observed in the Raman spectrum.

4. Conclusions

In this study, we employed the vertical Bridgman-Stockbarger technique to synthesize large, single-phase, stoichiometric BiSBr crystals. The structural analysis revealed a highly anisotropic, one-dimensional configuration, characterized by needle-like double chains stabilized by weak van der Waals forces. XPS measurements indicated a pristine surface devoid of oxidation in cleaved samples from the BiSBr ingot, with core-level peaks confirming the 1:1:1 stoichiometry and the valences of Bi^{3+}, S^{2-}, and Br^{-}. Further spectroscopic studies, supported by the existing literature, have elucidated strong covalent Bi-S bonds and relatively weaker Bi-Br bonds, with no detectable chemical bonds between S and Br. This aligns with a semi-ionic model, enhancing the understanding of the chemical structure of this material. Comparative analysis with analogous materials demonstrates that elemental substitutions within BiSBr are expected to maintain the chain structure, thus providing avenues to modify its optical or electrical properties. Cation substitution or doping is expected to significantly influence the BiSBr structure and can induce two-mode behavior in Raman spectra, which suggests notable changes to the vibrational properties. Conversely, anion substitution will have a lesser impact, offering a versatile method to tune the properties of BiSBr to meet specific functional requirements in advanced device applications.

CRediT authorship contribution statement

R. Sereika: Writing – original draft, Validation, Supervision, Investigation, Formal analysis, Data curation, Conceptualization. **Š. Varnagiris:** Writing – review & editing, Software, Investigation, Formal analysis. **M. Urbonavičius:** Writing – review & editing, Software, Investigation, Formal analysis. **R. Žaltauskas:** Writing – review & editing, Visualization, Resources, Methodology, Investigation, Formal analysis. **D. Milčius:** Validation, Resources, Project administration, Funding acquisition, Formal analysis.

Declaration of competing interest

The authors declare that they have no known competing financial interests or personal relationships that could have appeared to influence the work reported in this paper.

Data availability

Data will be made available on request.

References

[1] E. Dönges, Über Chalkogenohalogenide des dreiwertigen Antimons und Wismuts. I. Über Thiohalogenide des dreiwertigen Antimons und Wismuts, Z. Amorg. Allg. Chem. 263 (1950) 112–132, https://doi.org/10.1002/zaac.19502630113.

[2] D.V. Chepur, D.M. Bercha, I.D. Turyanitsa, V.Y. Slivka, Pecularities of the energy spectrum and edge absorption in the chain compounds $A^{V}B^{VI}C^{VII}$, Phys. Stat. Sol. 30 (1960) 461–468, https://doi.org/10.1002/pssb.19680300206.

[3] G.P. Voutsas, P.J. Rentzeperis, The crystal structure of bismuth sulfide bromide, BiSBr, Z. Kristallogr. 166 (1984) 153–158, https://doi.org/10.1524/zkri.1984.166.14.153.

[4] T. Inushima, X-ray study of crystal structure and diffuse scattering spectra of ferroelectric SbSBr having pseudo-Jahn–Teller phase transition, J. Phys. Chem. Solid 60 (1999) 587–598, https://doi.org/10.1016/S0022-3697(98)00321-7.

[5] R. Sereika, R. Žaltauskas, V. Lapeika, S. Stanionytė, R. Juškėnas, Structural changes in chlorine-substituted SbSI, J. Appl. Phys. 126 (2019) 114101, https://doi.org/10.1063/1.5117334.

[6] E. Wlaźlak, A. Blachecki, M. Bisztyga-Szklarz, S. Klejna, T. Mazur, K. Mech, K. Pilarczyk, D. Przyczyna, M. Suchecki, P. Zawalad, K. Szaciłowski, Heavy pnictogen chalcohalides: the synthesis, structure and properties of these rediscovered semiconductors, Chem. Commun. 54 (2018) 12133, https://doi.org/10.1039/c8cc05149f.

[7] P. Govindaraj, K. Murugan, K. Venugopal, One-dimensional van der Waals BiSBr: an anisotropic thermoelectric mineral, PCCP 26 (2024) 7124–7136, https://doi.org/10.1039/d3cp05849b.

[8] X. Guo, Y.-T. Huang, H. Lohan, J. Ye, Y. Lin, J. Lim, N. Gauriot, S.J. Zelewski, D. Darvill, H. Zhu, A. Rao, I. McCullocha, R.L.Z. Hoye, Air-stable bismuth sulfobromide (BiSBr) visiblelight absorbers: optoelectronic properties and potential for energy harvesting, J. Mater. Chem. A 11 (2023) 22775–22785, https://doi.org/10.1039/d3ta04491b.

[9] M.M. Frutos, M.E.P. Barthaburu, L. Fornaro, I. Aguiar, Bismuth chalcohalide-based nanocomposite for application in ionising radiation detectors, Nanotechnology 31 (2020) 225710, https://doi.org/10.1088/1361-6528/ab7675.

[10] S. Li, Z. Huang, Y. Ding, C. Zhang, J. Yu, Q. Feng, J. Feng, Growth of BiSBr microsheet arrays for enhanced photovoltaics performance, Small 19 (2023) 2306964, https://doi.org/10.1002/smll.202306964.

[11] A. Audzijonis, R. Sereika, R. Žaltauskas, A. Rėza, Optical properties of BiSBr and BiSeBr crystals, J. Phys. Chem. Solid 72 (2011) 1501–1505, https://doi.org/10.1016/j.jpcs.2011.09.010.

[12] A. Audzijonis, R. Sereika, Electronic structure and electron charge density in the interatomic bonds of BiSBr and BiSeBr crystals, Int. J. Mod Phys B 27 (2013) 1350122, https://doi.org/10.1142/S0217979213501221.

[13] J.M. Booth, M.V. Klymenko, J.H. Cole, S.P. Russo, Accurate calculation of excitonic signatures in the absorption spectrum of BiSBr using semiconductor Bloch equations, Phys. Rev. B 103 (2021) 115203, https://doi.org/10.1103/PhysRevB.103.115203.

[14] Z. Ran, X. Wang, Y. Li, D. Yang, X.-G. Zhao, K. Biswas, D.J. Singh, L. Zhang, Bismuth and antimony-based oxyhalides and chalcohalides as potential optoelectronic materials, Npj Comput Mater. 4 (2018) 14, https://doi.org/10.1038/s41524-018-0071-1.

[15] H. Kunioku, M. Higashi, R. Abe, Low-temperature synthesis of bismuth chalcohalides: candidate photovoltaic materials with easily, continuously controllable band gap, Sci. Reports 6 (2016) 32664, https://doi.org/10.1038/srep32664.

[16] D. Quarta, S. Toso, R. Giannuzzi, R. Caliandro, A. Moliterni, G. Saleh, A.-L. Capodilupo, D. Debellis, M. Prato, C. Nobile, V. Maiorano, I. Infante, G. Gigli, C. Giannini, L. Manna, C. Giansante, Colloidal bismuth chalcohalide nanocrystals, Angew. Chem. Int. Ed. 61 (2022) e202201747.

[17] U.V. Ghorpade, M.P. Suryawanshi, M.A. Green, T. Wu, X. Hao, K.M. Ryan, Emerging chalcohalide materials for energy applications, Chem. Rev. 123 (2023) 327–378, doi: acs.chemrev.2c00422.

[18] J. He, X. Hu, Z. Liu, W. Chen, G. Longo, Prospect for bismuth/antimony chalcohalides-based solar cells, Adv. Funct. Mater. 23 (2023) 2306075, https://doi.org/10.1002/adfm.202306075.

[19] B.H. Toby, R.B. Von Dreele, GSAS-II: the genesis of a modern open-source all purpose crystallography software package, J. Appl. Cryst. 46 (2013) 544–549, https://doi.org/10.1107/S0021889813003531.

[20] A.M. Ganose, K.T. Butler, A. Walsh, D.O. Scanlon, Relativistic electronic structure and band alignment of BiSI and BiSeI: candidate photovoltaic materials, Mater. Chem. A 4 (2016) 2060, https://doi.org/10.1039/c5ta09612j.

[21] A.M. Ganose, M. Cuff, K.T. Butler, A. Walsh, D.O. Scanlon, Interplay of orbital and relativistic effects in bismuth oxyhalides: BiOF, BiOCl, BiOBr, and BiOI, Chem. Mater. 28 (2016) 1980–1984, https://doi.org/10.1021/acs.chemmater.6b00349.

[22] T.P. Debies, J.W. Rabalais, X-ray photoelectron spectra and electronic structure of Bi_2X_3 (X = O, S, Se, Te), Chem. Phys. 20 (1977) 277–283, https://doi.org/10.1016/0301-0104(77)85033-7.

[23] A.V. Semencha, M.V. Kurushkin, V.A. Markov, A.L. Shakhmin, Vitreous arsenic sulfide doped with bismuth bromide, Tech. Phys. Lett. 41 (2015) 429–432, https://doi.org/10.1134/S1063785015050119.

[24] C. Cao, G. Xiao, Y. Lu, Humidity sensor based on BiOBr synthesized under ambient condition, J. Semicond. 43 (2022) 124101, https://doi.org/10.1088/1674-4926/43/12/124101.

[25] J. Grigas, E. Talik, M. Adamiec, V. Lazauskas, V. Nelkinas, XPS and electronic structure of quasi-one-dimensional BiSI crystals, J. Electron Spectros. Relat. Phenomena 153 (2006) 22–29, https://doi.org/10.1016/j.elspec.2006.06.001.

[26] J. Grigas, E. Talik, V. Lazauskas, X-Ray Photoelectron spectroscopy of ferroelectrics, Ferroelectrics 347 (2007) 86–100, https://doi.org/10.1080/00150190601187237.

[27] R. Sereika, R. Žaltauskas, Š. Varnagiris, M. Urbonavičius, F. Liu, Y. Ding, D. Milčius, On the structure of SbTeI, J. Appl. Phys. 132 (2022) 015106, https://doi.org/10.1063/5.0090152.

[28] M.K. Teng, M. Balkanski, M. Massot, M.K. Ziolkiewicz, Optical phonon analysis in the $A_VB_{VI}C_{VII}$ compounds, Phys Stat. Sol. (b) 62 (1974) 173, https://doi.org/10.1002/pssb.2220620117.

[29] M.K. Teng, M. Massot, M. Balkanski, S. Ziolkiewicz, Atomic substitution and ferroelectric phase transition in $Bi_xSb_{1-x}SI$, Phys. Rev. B 17 (1978) 3695, https://doi.org/10.1103/PhysRevB.17.3695.

[30] R.A. Groom, A. Jacobs, M. Cepeda, R. Drummey, S.E. Latturner, Structural, optical properties, Of Sb-substituted BiSI grown from sulfur/iodine flux, Inorg. Chem. 56 (2017) 12362–12368, https://doi.org/10.1021/acs.inorgchem.7b01839.

[31] R. Sereika, R. Žaltauskas, S. Bandaru, F. Liu, A. Čerškus, Two-transition behavior in $Bi_{0.5}Sb_{0.5}SeI$ crystals, J. Phys. Chem. Solid 154 (2021) 110031, https://doi.org/10.1016/j.jpcs.2021.110031.

[32] R. Nie, J. Im, S.I. Seok, Efficient solar cells employing light-harvesting $Sb_{0.67}Bi_{0.33}SI$, Adv. Mater. 31 (2019) 1808344, https://doi.org/10.1002/adma.201808344.

[33] E. Furman, O. Brafman, J. Makovsky, Phonons and ferroelectric phase transitions in SbSBr and SbSI and their solid solutions, Phys. Rev. B 8 (1973) 2341, https://doi.org/10.1103/PhysRevB.8.2341.